Chapter 9
Beam Instrumentation

A. Jansson, V. Lebedev, R. Moore, and V. Shiltsev

Operation of a superconducting magnet hadron collider, like Fermilab's Tevatron, requires a great deal of care, understanding of beam conditions, and trust in the beam diagnostics, because comparatively innocent little imperfections can lead to either beam blow-up and luminosity loss or to beam loss and quench of superconducting magnets. In the Tevatron such a quench results in 2–4 h of magnet recovery time and up to 8–16 h of no-luminosity time needed to produce the antiprotons needed for the next high energy physics (HEP) store. Over 8 years of operations we witnessed machine downtimes due to 0.5–1 % of beam intensity loss, poor beam lifetime, 0.5–1 mm orbit error, collimator malfunctioning, sequencer error, excursions of tunes or coupling of the order of few 0.001 or several units of chromaticity, instability occurrences, or malfunctioning of kickers, separators, or one of hundreds of power supplies, etc.—a detailed discussion can be found in [1]. Naturally, these peculiarities were reflected in the kinds of beam diagnostics we developed (e.g., minimization of their invasiveness) and the way they were exploited (fast data-logging, convenience for postmortem analysis, etc.).

Challenges in operation of the room-temperature accelerators in the proton injector chain machines are of a different sort and mostly related to necessity of tight control of beam losses in order to keep residual level of beam-induced radiation under certain limit, usually under 1 W/m. In addition, antiproton production, accumulation, and cooling require reliable diagnostics of low intensity beams and very slow beam cooling processes.

A. Jansson • V. Lebedev • R. Moore • V. Shiltsev (✉)
Accelerator Physics Center, Fermi National Accelerator Laboratory, MS221, PO Box 500, Batavia, IL 60510, USA
e-mail: val@fnal.gov; shiltsev@fnal.gov

V. Lebedev and V. Shiltsev (eds.), *Accelerator Physics at the Tevatron Collider*, Particle Acceleration and Detection, DOI 10.1007/978-1-4939-0885-1_9,

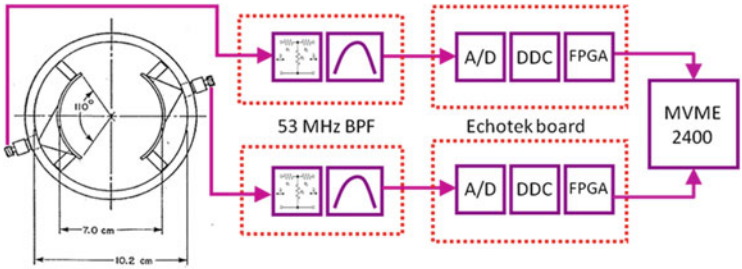

Fig. 9.1 Block diagram of the upgraded Tevatron BPM electronics. Signals from the BPM pickups go through a 53 MHz bandpass filter before being digitized and down-converted on an Echotek model ECDR-GC814-FV-A digital receiver board. A Motorola MVME-2400 processor provides the interface to ACNET for BPM readings and configuration control [1]

9.1 Beam Position Monitors

In the Tevatron, the protons and antiprotons circulate within a single beam pipe, so electrostatic separators are used to kick the beams onto distinct helical orbits to allow head-on collisions only at the desired interaction points. At 150 GeV, separation is limited to ~10–22 mm by physical aperture, while the separation above 600 GeV, ~3–6 mm, is limited by the breakdown (spark) rate of the separators at high voltage. Long-range beam effects degrade beam lifetime and machine performance, and having a good model of the optics is essential to understanding problems and how to improve operations. Reliable beam position monitors (BPMs) with good resolution are needed to measure the optics and construct the model (see chap. 2).

There were several problems with the BPM system developed for the Collider Run I [2] that hampered machine operations and diagnosis of possible problems in the Collider Run II. The orbit would deviate significantly from the desired reference orbit, 0.5 mm RMS (root mean square) differences in only 1–2 weeks, so global orbit smoothing was needed regularly. The BPM response to coalesced beam (a transfer concentrated in a single 53 MHz bucket, used for HEP stores) and uncoalesced beam (30 or so consecutive buckets, used for tune-up) differed enough so that a direct comparison between orbits recorded during HEP stores could not be compared easily to proton-only stores used to tune the machine or do orbit smoothing. The BPM position resolution was only ~150 μm and limited optics measurements to at best 20 % uncertainty. The turn-by-turn (TBT) capability was unreliable, and the system was blind to antiprotons. All these issues motivated the decision to upgrade the BPM electronics and take advantage of current technology [3]. The 240 Tevatron BPM pickups remained unchanged.

Figure 9.1 shows a block diagram of the upgraded BPM electronics system. A cross-sectional view of the pickup is shown on the left. Each detector has two 18 cm long copper electrodes in a 10.2 cm diameter stainless steel pipe. Each electrode is bent to a 3.5 cm radius of curvature, and subtends 110° of arc for a

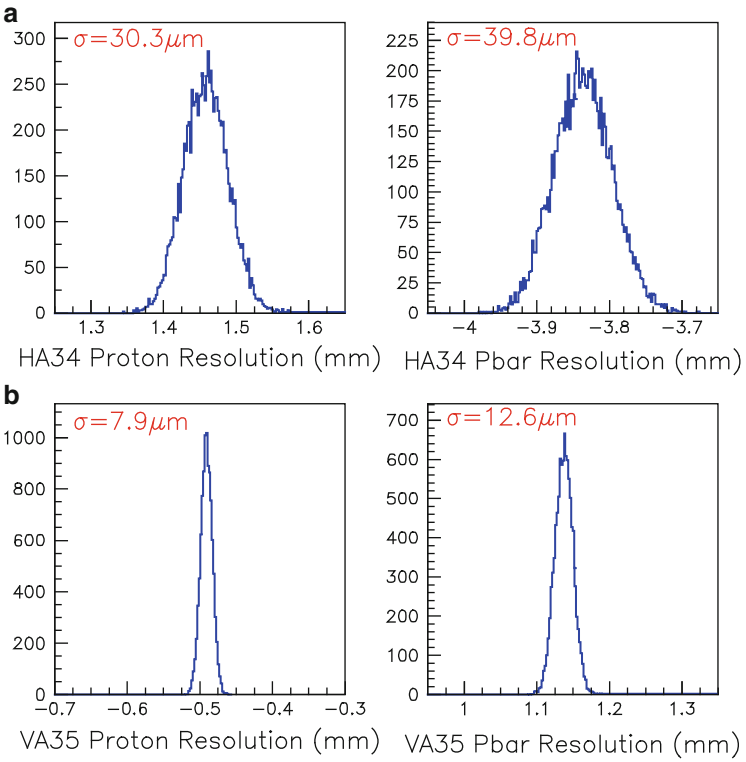

Fig. 9.2 (**a**) (*top*) Simultaneous horizontal position measurements from one BPM for protons (*left*) and antiprotons (*right*). (**b**) (*bottom*) Simultaneous vertical position measurements from one BPM for protons (*left*) and antiprotons (*right*). The given RMS values include all effects: resolution of the BPM and electronics, real beam motion (especially synchrotron oscillations for the horizontal data), and imperfect cancellation of the proton contamination into the antiproton signal [1]

centered beam. The available aperture is about 7 cm, the same as the accelerator beam pipe. The arc length and the spacing from the wall of the stainless steel pipe were selected to provide a uniform position response (including lack of sensitivity to motion in the orthogonal plane), while rigorously maintaining a 50 Ω transmission line impedance. RG-8 coaxial cables carry the signals from both ends of each pair of BPM pickups to VME racks in service buildings. In the VME crate are analog filter boards (53 MHz bandpass and attenuation), Echotek 8-channel 80 MHz digital receiver boards (ECDR-GC814-FV-A), as well as a Motorola MVME-2400 processor and a module providing clock and trigger signals. The new electronics were installed and commissioned bit by bit, usually between HEP stores, so that only a small number of BPMs would be affected at any one time. This strategy minimized the impact on operations and led to a successful implementation of the new system.

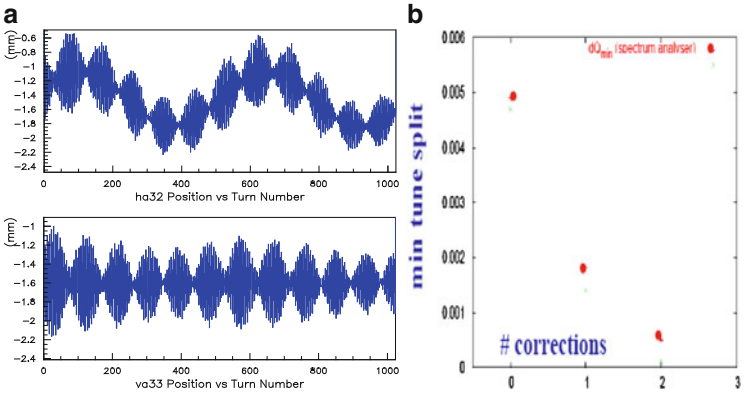

Fig. 9.3 (**a**) (*left*) Example of turn-by-turn measurements (*top*—horizontal, *bottom*—vertical) from the upgraded BPM electronics after intentionally kicking the proton beam. (**b**) (*right*) Measurements of minimum tune split during attempts to reduce coupling during machine tune-up. The *red points* are data from tune measurements made by looking at Schottky signals using a spectrum analyzer, while the *green points* are derived from turn-by-turn BPM measurements after kicking the beam. The turn-by-turn measurements achieve better results more quickly and more reliably than the spectrum analyzer method [1]

An example of the improved resolution of the new BPM electronics is shown in Fig. 9.2. The plots show distributions of the proton and antiproton closed orbit position measurements for one horizontal and one vertical BPM. The noted RMS values include the effects of true beam motion, e.g. synchrotron oscillations, and the imperfect cancellation of the proton signal onto the signal from the smaller intensity antiprotons. The intrinsic resolution from the BPMs themselves is ≈5 μm, much better than the 150 μm resolution of the old system.

The new electronics provide up to 8192 TBT position measurements at injection and on-demand. Figure 9.3 shows TBT measurements from one horizontal and one vertical BPM after intentionally kicking the beam horizontally in order to measure coupling during machine tune-up. The effect from coupling and synchrotron oscillations are clearly visible. The TBT capabilities are being exploited to develop faster and more reliable methods of measuring and correcting the beam optics.

The improved resolution of the BPMs has allowed better measurements of the machine optics which has led to lattice corrections and improvements [4, 5]. For example, the beta-functions can be measured to better than 5 % accuracy, and a new low-beta lattice with smaller $\beta^* = 28$ cm was created and increased luminosity by ≈10 %.

We have observed significant beam orbit motion during stores caused by motion of the low-beta quadrupoles and have been able to understand the source and implement an automated orbit-smoothing algorithm [6] that keeps the orbit from wandering during stores (see Fig. 9.4). In addition, the BPM response no longer

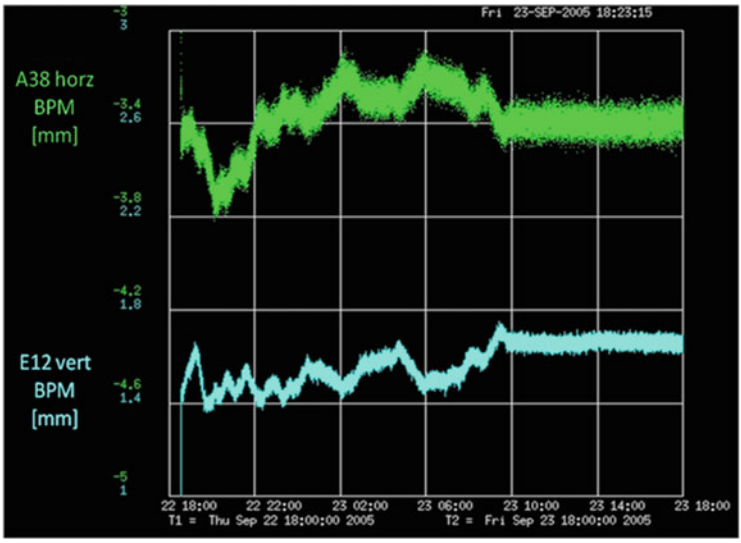

Fig. 9.4 Proton beam positions from a horizontal BPM (*top*) and a vertical BPM (*bottom*) over a 24-hour period during a high-energy physics store. The vertical scale is 400 μm per division. Before an orbit stabilization algorithm was enabled at 10:00, the orbit could wander by over 400 μm in a short period. After orbit stabilization was turned on, the orbit drift was reduced successfully to less than 50 μm. The algorithm uses several dipole correctors near the interaction regions to counteract motion of the low-beta quadrupoles caused by thermal and pressure differences between the Tevatron tunnel and the experimental halls [1]

depends on the bunch structure, so we can use orbit data from HEP stores to make global orbit corrections when needed.

9.2 Diagnostics for Low-Beta Quadrupoles and IPs

As mentioned above in Chapter 2.4, vibrations of low-beta quadrupoles are primarily responsible for orbit oscillations in the Tevatron, so we equipped each of the magnets with a fast 1 μrad resolution tiltmeter and 0.1 μm resolution hydrostatic level sensors (HLS) to detect vertical motion [7].

Some remarkable examples of orbit and magnet vibrations excited by fire trucks passing by the CDF building and remote earthquakes are shown in Fig. 9.5a, b. The HLS systems also track magnet motion due to continuous sinking of the CDF detector with rate of 0.25–0.5 mm/year. Such movements lead to a slow drift of the interaction point (IP) position inside the CDF silicon vertex detector (SVX). This and other beam-related information (like loss rates of various counters) can be monitored by Tevatron operators and physicists. For example, both CDF and D0 detectors provide data on the beta-functions at the IPs [8] (see Fig. 9.6) which is very helpful and

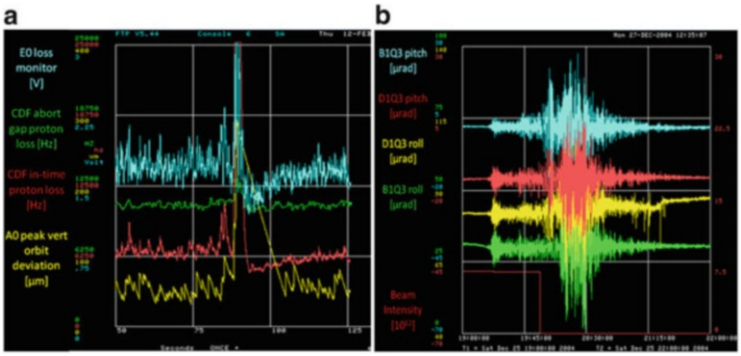

Fig. 9.5 (**a**) (*left*) 200 μm orbit oscillations, beam losses, and low-beta quadrupole vibrations excited by a 40,000 lb fire truck passing near the CDF Detector Hall. The effect was greatly reduced after installation of new quad girder supports in the 2005 shutdown; (**b**) (*right*) Disastrous M8.9 earthquake in Sumatra December 25, 2004 resulted in ±50 μrad motion as seen by the tiltmeters on CDF and D0 low-beta quadrupoles. The Tevatron beam (lower *red line* with a step down) was intentionally terminated before the arrival of the S-wave. The event lasted over 2 h [1]

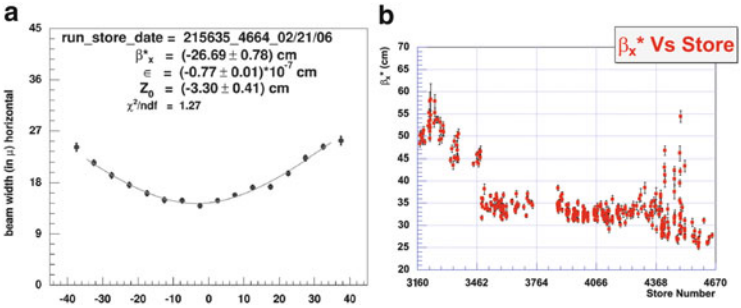

Fig. 9.6 (**a**) (*left*) RMS horizontal width of D0 luminous region vs longitudinal position. The parabolic fit is for hour-glass effect with $\beta^*_x = 27$ cm; (**b**) (*right*) January 2004–March 2006 history of the horizontal beta-function at the D0 IP measured by the D0 silicon vertex detector [1]

provides an additional insight into beam collision effects. Vertex analysis also allows separate determination of the proton and antiproton RMS bunch lengths [9].

9.3 Schottky Monitors

Measuring Schottky noise is a powerful nondestructive diagnostic for the Tevatron accelerators. It can be used for both continuous and bunched beams, in transverse and longitudinal degrees of motion, and for determination of a number of important beam parameters.

9.3.1 Schottky Noise in Continuous Beam

We start our consideration from the continuous beam. For the case of non-overlapping Schottky bands the spectral density of fluctuations of the beam current in the pickup in vicinity of n-th harmonic is [10]:

$$P_n(\delta\omega_n) = \frac{1}{\varepsilon_n(\delta\omega_n)} \frac{e^2 f_0 N \psi(\delta\omega_n/\omega_0 n\eta)}{2\pi|n\eta|}, \qquad \delta\omega_n = \omega_0 n\eta \frac{\Delta p}{p}. \tag{9.1}$$

Here N is the number of particles in the beam, $\eta = \alpha - 1/\gamma^2$ is the slip factor, $f_0 = \omega_0/2\pi$ is the revolution frequency, $\Delta p/p$ is the relative momentum deviation, and $\varepsilon_n(\delta\omega_n)$ is the beam dielectric function describing particle interaction. We also assume that the particle distribution function, $\psi(\Delta p/p)$, is normalized to 1, $\int \psi(x)\, dx = 1$, and that the spectral density and the correlation function are related by the following equation:

$$K_n(\tau) \equiv \langle I_n(t)^* I_n(t+\tau)\rangle_t = \int_{-\infty}^{\infty} P_n(\omega) \mathrm{e}^{i\omega\tau} d\omega. \tag{9.2}$$

Here $I_n(t)$ is the complex amplitude of the beam current fluctuations, and * denotes a complex conjugate. The magnitude of beam current fluctuations has a Gaussian distribution:

$$f_I(|I|) = \frac{|I|}{K_n(0)} \exp\left(-\frac{|I|^2}{K_n(0)}\right), \tag{9.3}$$

while the rate at which the amplitude and phase of fluctuations are changing is determined by the correlation function of Eq. (9.2). It is assumed in Eq. (9.3) that the harmonic number takes both positive and negative values, $n = -\infty, \ldots \infty$. If one considers only positive n, the result of Eq. (9.3) has to be multiplied by factor of 2.

If the particle interaction is sufficiently small at the revolution harmonic where measurements are performed, the beam dielectric function is close to 1 and it can be neglected in Eq. (9.1). In this case the beam longitudinal distribution is proportional to the spectral density of beam current fluctuations. If, however, the particle interaction cannot be neglected, the analysis of the beam spectra becomes much more complicated task. For a low energy machines their longitudinal impedance is dominated by the beam space charge impedance. In this case $|Z_n/n|$ stays constant up to very high frequency, $\omega \approx \pi c\gamma/a$, and beam interaction is equally strong for all harmonics. Here a is the vacuum chamber radius, and γ is the relativistic factor. However for high energy machines $|Z_n/n|$ is usually decreasing with frequency and therefore measurements at higher frequencies can reduce an effect of particle interaction. The first work devoted to the extraction of beam parameters from the longitudinal Schottky noise of deeply cooled beam, where Schottky spectrum is

completely dominated by particle interaction, was reported in [11]. Below we assume that the particle interaction is sufficiently small and can be neglected.

A choice of data acquisition technique used for measurement of beam spectrum depends on time available for measurements. If time is large enough, a general purpose scanning spectrum analyzer addresses the problem. If time allocated for a measurement is small, the beam signal is usually down-converted to a smaller frequency where a vector signal analyzer (VSA) can be used. If the beam distribution changes fast, the process is not repeatable, and a detailed evolution of beam distribution is desired, a direct digitization of down-converted beam noise by fast ADC with subsequent digital Fourier transform can be a better choice. In this case the entire process is recorded to a single data array resulting in no loss of information. After the measurements the data are split into smaller arrays, and the Fourier transform is performed for each of them. After averaging of nearby spectra one finally obtains a sequence of spectra representing an evolution of particle distribution.

Let us estimate the time required for a single measurement of the distribution function. Let the noise be digitized with sampling rate f_s. After the measurement the data are split into M arrays of length N; each array is subjected to a digital Fourier transform and corresponding spectral densities of the beam noise are computed for each array, $S_n = |a_n|^2$; and finally the obtained M spectral densities are summed to find an average. Such procedure determines that the maximum frequency in the spectrum is $f_s/2$, and the frequency resolution is f_s/N. After Fourier transform the complex amplitude of each harmonic, a_n, has a random values of phase and amplitude. The distribution over phase is uniform, and the distribution for modules of squared amplitudes, $|a_n|^2$, is described by Eq. (9.3). Typically the frequency resolution, $\delta f = f_s/N$, is chosen to be much smaller than a width of the spectrum $\Delta\omega$. In this case the decoherence time, $\sim 1/\Delta\omega$, is smaller than the time required to sample one array, $1/\delta f$, and, consequently, amplitudes of each next spectrum are statistically independent. Therefore the final spectral density obtained by averaging of M initial spectral densities has a relative value of statistical fluctuations equal to $1/\sqrt{M}$. Thus we finally obtain that the time required to obtain the distribution function with relative accuracy $\sqrt{\langle \delta\psi^2 \rangle}/\psi$ is:

$$T = \frac{1}{\Delta\omega} \frac{\Delta\omega}{\delta f} \frac{1}{\langle \delta\psi^2 \rangle / \psi^2}. \tag{9.4}$$

For a typical measurement the accuracy is ~10 % ($M = 100$) and a relative frequency resolution $\delta f/\Delta\omega \approx 0.06/(2\pi) \approx 0.01$. That results in that the required time is $\approx 10^4/\Delta\omega$. That determines that the measurement time is inversely proportional to the harmonic number.

In difference to the longitudinal Schottky noise taking place at the revolution harmonics the transverse Schottky noise comes at sidebands of the betatron frequencies, $\omega_{\perp n} = \omega_0(n + Q)$. For the case of non-overlapping Schottky bands the effective spectral density of beam current transverse noise is:

$$P_{\perp n}(\delta\omega_{\perp n}) = \frac{1}{\varepsilon_{\perp n}(\delta\omega_{\perp n})} \frac{e^2 f_0 N \psi(\delta\omega_{\perp n}/\omega_0(n\eta+\xi))}{2\pi|n\eta+\xi|} \frac{\overline{x^2}}{A^2}, \quad \delta\omega_{\perp n}$$
$$= \omega_0(n+Q)\frac{\Delta p}{p}, \tag{9.5}$$

where we assume that the transverse distribution does not depend on the momentum, $\sqrt{\overline{x^2}}$ is the rms value of particle transverse motion (in x- or y-plane), A is the effective aperture of pickup, Q is the betatron tune, and ξ is the tune chromaticity. The transverse Schottky noise is completely determined by the rms particle amplitude in the pickup and is not coupled to the details of transverse particle distribution. For high frequencies, $f/f_0 \gg \xi/\eta$, where the Schottky noise is less affected by particle interaction the distribution width is determined rather by the revolution frequency spread than by the betatron frequency spread. The noise integral over one transverse Schottky band is directly related to the rms beam size and, consequently, to the beam emittance; and the difference of widths for the positive and negative sidebands, $(n \pm Q)\, f_0$, (also called lower and upper sidebands) is directly related to the tune chromaticity:

$$\xi = n\eta \frac{\Delta f_+ - \Delta f_-}{\Delta f_+ + \Delta f_-}. \tag{9.6}$$

Here Δf_+ and Δf_- are the Schottky band widths for positive and negative betatron bands. Thus, measurements of transverse Schottky noise yield simple and noninvasive measurements of the beam emittance and the tune chromaticity.

9.3.2 Longitudinal Schottky Noise in Bunched Beam

In difference to the continuous beam the electromagnetic signal of bunched beam consists of two parts: the bunch coherent signal (observed on the revolution frequency harmonics) and the incoherent signal of particles (observed in vicinity of these harmonics).

Firstly, let us consider the spectrum of a single particle. We assume that the particle performs a synchrotron motion so that its position relative to the bunch center is described by a periodic function $z(t)$ with period $T_s = 2\pi/\omega_s$. Then, the spectrum of particle current is:

$$S(\omega) = \frac{e}{2\pi}\int_{-\infty}^{\infty} dt e^{-i\omega t} \sum_{n=-\infty}^{\infty} \delta\left(t - nT_0 - \frac{z(nT_0)}{\beta c}\right)$$
$$= \frac{e}{2\pi}\sum_{n=-\infty}^{\infty} \exp\left(-i\omega\left(nT_0 + \frac{z(nT_0)}{\beta c}\right)\right). \tag{9.7}$$

Here to find the time of pickup crossing by the particle we assumed that the synchrotron tune is small, $\nu_s \equiv \omega_s/\omega_0 \ll 1$. To compute the sum in the right-hand part of Eq. (9.7) we expand the exponential term in the Fourier series:

$$\exp\left(-i\frac{\omega z(t)}{\beta c}\right) = \sum_{m=-\infty}^{\infty} z_m \mathrm{e}^{im\omega_s t}, \quad z_m = \frac{1}{T_s}\int_{-T_s/2}^{T_s/2} \exp\left(-i\frac{\omega z(t)}{\beta c}\right)\mathrm{e}^{-im\omega_s t}dt. \tag{9.8}$$

Substituting Eq. (9.8) into Eq. (9.7) and using the following identities,

$$\sum_{n=-\infty}^{\infty} \exp(ixn) = 2\pi \sum_{n=-\infty}^{\infty} \delta(x - 2\pi n), \quad \int \delta(ax)dx = \frac{1}{a}\int \delta(x)dx, \tag{9.9}$$

we finally obtain:

$$S(\omega) = \frac{e}{T_0}\sum_{n=-\infty}^{\infty}\sum_{m=-\infty}^{\infty} z_m \delta(\omega - n\omega_0 - m\omega_s). \tag{9.10}$$

The beam current in the pickup can be presented as a sum of currents of individual particles:

$$I(t) = e\sum_k \sum_{n=-\infty}^{\infty} \delta\left(t - nT_{0_k} - \frac{z_k(nT_{0_k})}{\beta c}\right),$$

where the index k numerates particles (from 1 to N_p), and we assume that different particles have different synchrotron amplitudes, phases, and periods. Performing the inverse Fourier transform of each particle spectrum [see Eq. (9.10)] one obtains:

$$I(t) = e\sum_k \sum_{n=-\infty}^{\infty}\sum_{m=-\infty}^{\infty} \frac{z_{m_k}}{T_{0_k}} \exp(i(n\omega_{0_k} + m\omega_{s_k})t). \tag{9.11}$$

In the further consideration we will neglect the difference in particle periods in the denominator in the right-hand side of Eq. (9.11) ($T_{0k} \to T_0$). Taking into account the relationship between the spectral density of beam current and its correlation function:

$$P(\omega) = \frac{1}{2\pi}\int_{-\infty}^{\infty} K(\tau)\mathrm{e}^{-i\omega\tau}d\tau. \tag{9.12}$$

We obtain for the beam spectral density:

$$P(\omega) = \frac{e^2}{2\pi {T_0}^2}\int_{-\infty}^{\infty} \mathrm{e}^{-i\omega\tau} d\tau \sum_{k,l=-\infty}^{\infty}\sum_{n,p=-\infty}^{\infty}\sum_{m,q=-\infty}^{\infty} \left\langle z_{m_k} {z_{q_l}}^* \exp(i(n\omega_0 + m\omega_{s_k})t)\exp(-i(p\omega_0 + q\omega_{s_l})(t+\tau))\right\rangle_t$$
$$= \frac{e^2}{2\pi {T_0}^2}\int_{-\infty}^{\infty} \mathrm{e}^{-i\omega\tau} d\tau \sum_{k,l=-\infty}^{\infty}\sum_{n,p=-\infty}^{\infty}\sum_{m,q=-\infty}^{\infty} \exp(-i(p\omega_0 + q\omega_{s_l})\tau)\left\langle z_{m_k} {z_{q_l}}^* \exp(i((n-p)\omega_0 + (m\omega_{s_k} - q\omega_{s_l}))t)\right\rangle_t, \tag{9.13}$$

where * denotes the complex conjugate, and $\langle \ldots \rangle_t$ denotes the averaging over time and initial distributions. The averaging over t leaves in the sum only terms with $k = l$ and $n = p$ if both m and q are not equal to zero. For $m = q = 0$ and $n = p$ all terms with $k \neq 1$ also contributes. That yields:

$$P(\omega) = \frac{e^2}{2\pi {T_0}^2}\int_{-\infty}^{\infty} \mathrm{e}^{-i\omega\tau} d\tau \left[\sum_{k,l=-\infty}^{\infty}\sum_{n=-\infty}^{\infty} \langle z_{0_k} {z_{0_l}}^*\rangle \mathrm{e}^{-in\omega_0\tau} + \sum_{k=-\infty}^{\infty}\sum_{n=-\infty}^{\infty}\sum_{\substack{m=-\infty \\ m\neq 0}}^{\infty} \langle z_{m_k} {z_{m_k}}^*\rangle \mathrm{e}^{-i\left(n\omega_0 + m\omega_{s_k}\right)\tau}\right]. \tag{9.14}$$

After integration one obtains:

$$P(\omega) = \frac{e^2}{{T_0}^2}\left[\sum_{k,l}\sum_{n=-\infty}^{\infty} \langle z_{0_k} {z_{0_l}}^*\rangle \delta(\omega - n\omega_0) + \sum_{k}\sum_{n=-\infty}^{\infty}\sum_{\substack{m=-\infty \\ m\neq 0}}^{\infty} \left\langle |z_{m_k}|^2\right\rangle \delta(\omega - n\omega_0 - m\omega_{s_k})\right]. \tag{9.15}$$

Note that Eq. (9.8) directly results in that for $m = 0$ the amplitude z_m is a positive real number which does not depend on the initial particle phase, while for $m \neq 0$ the amplitude is a complex number which argument depends on the initial phase of particle synchrotron motion. That yields that $z_{0_k} {z_{0_l}}^*$ is a real and positive number even for different particles ($k \neq l$). Averaging over initial distribution sets and replacing the summing in Eq. (9.15) by integration over the distribution finally results in:

$$P(\omega) = \frac{e^2}{{T_0}^2}\left[N_\mathrm{p}\left(N_\mathrm{p} - 1\right)\sum_{n=-\infty}^{\infty} \delta(\omega - \omega_{n0})\left|\int dJ z_0(J,\omega) f(J)\right|^2 + N_\mathrm{p}\sum_{n=-\infty}^{\infty}\sum_{m=-\infty}^{\infty}\int \delta(\omega - \omega_{nm})|z_m(J,\omega)|^2 f(J) dJ\right], \tag{9.16}$$

where $\omega_{nm} = n\omega_0 + m\omega_s(J)$, J is the action of longitudinal motion so that $\int f(J)\, dJ = 1$, N_P is the number of particles in the bunch,

$$z_m(J,\omega) = \frac{1}{T_s(J)} \int_{-T_s(J)/2}^{T_s(J)/2} \exp\left(-i\frac{\omega z(J,t)}{\beta c}\right) \mathrm{e}^{-im\omega_s(J)t} dt, \tag{9.17}$$

and the function $z(J, t)$ describes a dependence of longitudinal particle position on time. The first addend in Eq. (9.16) represents the coherent signal of the bunch, and the second one represents the incoherent signal or the Schottky noise. Taking into account large number of particles in the beam we omit 1 in the product $N_\mathrm{p}\,(N_\mathrm{p} - 1)$ in further consideration

Using Eqs. (9.9) and (9.17) one can easily prove that in the general case

$$\sum_{m=-\infty}^{\infty} |z_m(J,\omega)|^2 = 1. \tag{9.18}$$

Integrating the spectral density of Schottky noise [second addend of Eq. (9.16)] over one revolution harmonic one obtains:

$$\int_{(n-1/2)\omega_0}^{(n+1/2)\omega_0} P_{ic}(\omega) d\omega = \frac{e^2}{{T_0}^2} N_\mathrm{p} \int_{(n-1/2)\omega_0}^{(n+1/2)\omega_0} d\omega \sum_{m=-\infty}^{\infty} \int \delta(\omega - \omega_{nm}) |z_m(J)|^2 f(J) dJ = \frac{e^2}{{T_0}^2} N, \tag{9.19}$$

where Eq. (9.18) was used to perform the summation over m. One can see that the Schottky noise integral over one revolution harmonic does not depend on particle motion and is equal to the integral of Schottky noise of continuous beam with the same number of particles.

The coherent part of beam signal presented by the first addend in Eq. (9.16) can be expressed as sum of revolution frequency harmonics

$$P_c(\omega) = \frac{e^2}{{T_0}^2} {N_\mathrm{p}}^2 \sum_{n=-\infty}^{\infty} \delta(\omega - \omega_{n0}) |A_n|^2, \tag{9.20}$$

where coefficients A_n can be expressed as corresponding Fourier harmonics of bunch longitudinal density as follows from the string of equations below.

$$A_n = \int dJ z_0(J, n\omega_0) f(J) = \int dJ f(J) \frac{\omega_s(J)}{2\pi} \int_{-T_s(J)/2}^{T_s(J)/2} \exp\left(-i\frac{n\omega_0 z(J,t)}{\beta c}\right) dt$$
$$= \int dJ f(J) \frac{\omega_s(J)}{2\pi} 2 \int_{-z_{\max}(J)}^{z_{\max}(J)} \exp\left(-i\frac{n\omega_0 z}{\beta c}\right) \frac{dz}{(dz/dt)_I} = \int dz f_z(z) \exp\left(-i\frac{n\omega_0 z}{\beta c}\right). \tag{9.21}$$

Here the factor of 2 appearing at the transition from integration over t to z is related to the integration over half of synchrotron motion period for the integration over z, and we used the following equation relating distribution functions over action, $f(J)$, and over longitudinal coordinate, $f_z(z)$,

$$f_z(z) = \frac{1}{\pi} \int dJ \frac{f(J)\omega_s(J)}{(dz/dt)_I}, \tag{9.22}$$

where $\int f_z(z)\mathrm{d}z = 1$.

The second addend in Eq. (9.16) represents the incoherent part of beam signal. For sufficiently high frequencies it can be reduced to the form which directly relates the spectral density to the distribution function over momentum. In this case the major contribution to the integral of Eq. (9.17) comes from the area where

$$m\omega_s = -\frac{\omega}{\beta c} \frac{dz(J, t_r)}{dt}. \tag{9.23}$$

There are two points in one revolution period where this condition is satisfied. That yields that Eq. (9.17) can be approximated as following:

$$z_m(J,\omega) = \frac{1}{T_s(J)} \sum_{r=1,2} \exp\left(-i\left(\frac{\omega z(J,t_r)}{\beta c} + m\omega_s(J)\right)\right) \int_{-\infty}^{\infty} \exp\left(-i\frac{\omega}{2\beta c}\frac{d^2 z(J,t_r)}{dt^2}\tau^2\right) d\tau, \tag{9.24}$$

where time t_r is determined by Eq. (9.23). Here and below we do not imply the symmetry of potential well. For a symmetric potential well the modulus of $d^2z(J, t_r)/dt^2$ would be equal for both resonance points (r=1, 2). Performing integration and squaring the result one obtains:

$$|z_m(J,\omega)|^2 = \frac{2\pi}{T_s(J)^2} \frac{\beta c}{\omega} \sum_{r=1,2} \left|\frac{d^2 z(J,t_r)}{dt^2}\right|^{-1}, \tag{9.25}$$

where we omitted the interference term between two addends. This interference term oscillates fast with m and J and makes negligible contribution after averaging over distribution. Substituting Eq. (9.25) to Eq. (9.16) one obtains:

$$P_{ic}(\omega) = \frac{e^2}{{T_0}^2} N_{\mathrm{p}} \sum_{n=-\infty}^{\infty} \sum_{m=-\infty}^{\infty} \int \delta(\omega - \omega_0 n - \omega_s m) \frac{2\pi}{T_s(J)^2} \frac{\beta c}{\omega} \sum_{r=1,2} \left| \frac{d^2 z(J, t_r)}{dt^2} \right|^{-1} f(J) dJ. \tag{9.26}$$

At high frequencies the synchrotron number m is large and summing over m can be replaced by integration.[1] Introducing the momentum as $\widetilde{p} = dz(J,t)/dt$, replacing the integration variable m by $\widetilde{p}$ and using Eq. (9.23) one obtains:

$$P_{ic}(\omega) = \frac{2\pi e^2}{{T_0}^2} N_{\mathrm{p}} \sum_{n=-\infty}^{\infty} \int \frac{\omega}{\omega_s(J)} \frac{d\widetilde{p}}{\beta c} \int \delta\left(\omega\left(1 + \frac{\widetilde{p}}{\beta c}\right) - \omega_0 n\right)$$
$$\left(\frac{\omega_s(J)}{2\pi}\right)^2 \frac{\beta c}{\omega} \sum_{r=1,2} \left| \frac{1}{d\widetilde{p}(J, p_r)/dt} \right| f(J) dJ. \tag{9.27}$$

Taking into account that the distribution function over momentum is equal to

$$f_p(\widetilde{p}) = \frac{1}{2\pi} \int \sum_{r=1,2} \left| \frac{1}{d\widetilde{p}(J, \widetilde{p})/dt} \right| \omega_s(J) f(J) dJ, \tag{9.28}$$

and performing integration one finally obtains:

$$P_{ic}(\omega) = \frac{e^2}{{T_0}^2} N_{\mathrm{p}} \sum_{n=-\infty}^{\infty} f_p\left(\frac{n\omega_0 - \omega}{\omega_0 n} c\beta\right). \tag{9.29}$$

where $\int f_p(\widetilde{p}) d\widetilde{p} = 1$. Note that by definition the momentum $\widetilde{p}$ is related to the particle momentum deviation as $\widetilde{p} = R_0 \eta \omega_0 \Delta p/p$, where R_0 is the average machine radius.

Although the functional form of Eq. (9.16) is quite different from Eq. (9.1) the corresponding spectral densities are numerically close if frequency is sufficiently large as it follows from Eq. (9.29). To demonstrate the considered above formalism we consider Schottky spectra for cases of two quite different potential wells: (1) a barrier bucket with the rigid walls and (2) a parabolic well where particle motion is linear and the synchrotron frequency does not depend on frequency.

In the case of barrier bucket a dependence of particle position on time during one synchrotron period can be expressed in the following form:

[1] It implies that the resolution of the measurements is larger than the synchrotron frequency, ω_s, or sufficiently large dependence of synchrotron frequency on the action, J, so that an averaging over particle distribution makes a smooth spectral density.

$$z_m(\Delta p, t) = L_b\left(\left|\frac{2t}{T_s(\Delta p)}\right| - \frac{1}{2}\right), \quad |t| < \frac{T_s(\Delta p)}{2}, \tag{9.30}$$

where L_b is the span of longitudinal particle motion, $T_s(\Delta p) = 4\pi\kappa_b/(\omega_0\eta\Delta p/p)$ is the synchrotron period, $\kappa_b = L_b/2\pi R_0$ is the fraction of the orbit taken by the particle motion. Substituting Eq. (9.30) to Eq. (9.17) and performing integration at frequencies $\omega_{nm} = n\omega_0 + m\omega_s(\Delta p)$ one obtains the spectrum of a single particle motion:

$$z_{nm} = \mathrm{e}^{-i\pi m/2}\frac{\sin\left(\pi(m - 2\kappa_b n)/2\right)}{\pi(m - 2\kappa_b n)} + \mathrm{e}^{i\pi m/2}\frac{\sin\left(\pi(m + 2\kappa_b n)/2\right)}{\pi(m + 2\kappa_b n)}. \tag{9.31}$$

One can see that the amplitudes z_{nm} do not depend on $\Delta p/p$ but the spectrum width is proportional to $\omega_s(\Delta p)$ and, consequently, to $\Delta p/p$. In the case of continuous beam the single particle spectrum in vicinity of n-th harmonic is presented by a single line shifted by $n\omega_0\eta\Delta p/p$. In the case of particle in the barrier bucket the particle is moving back and forward with momentum deviation of $\pm\Delta p/p$ but instead of being presented by only two lines with frequency shifts $\pm n\omega_0\eta\Delta p/p$ its spectrum is presented by large number of lines. However for sufficiently large frequency, $2\kappa_b n \gg 1$, the relative width of this spectrum is narrow and the spectrum is peaked in vicinity of these two lines. For harmonic numbers above $n \gg 1/\kappa_b \equiv 2\pi R_0/L_b$ the spectrum of bunched beam is close to its momentum distribution.

In the case of parabolic potential well a dependence of particle position on time during one synchrotron period is:

$$z_m(\Delta p, t) = \frac{L_b}{2}\cos\left(\omega_s t\right). \tag{9.32}$$

Substituting it to Eq. (9.17) and performing integration one obtains the spectrum of a single particle motion:

$$z_{nm} = \mathrm{e}^{-i\pi m/2}J_m(\pi\kappa_b n), \tag{9.33}$$

where the same as for a beam in the barrier bucket, $\kappa_b = L_b/2\pi R_0$. A larger spectrum width for the case of parabolic well is related to the $\pi/2$ larger maximum momentum deviation for the same values of bunch length and synchrotron period. One can see that $|z_{nm}|$ is a fast oscillating function of m. However in practical applications the observed spectrum is created by signals of many particles having different amplitudes which effectively smears these fast oscillations in the spectrum. Applying Eq. (9.25) to the parabolic potential well one obtains the high frequency asymptotic

$$|z_{nm}|_{\mathrm{HF}}{}^2 = \frac{1}{\pi^2\kappa_b n\sqrt{1 - (m/\pi\kappa_b n)^2}}, \quad |m| < \pi\kappa_b n. \tag{9.34}$$

which describes the averaged distribution sufficiently well.

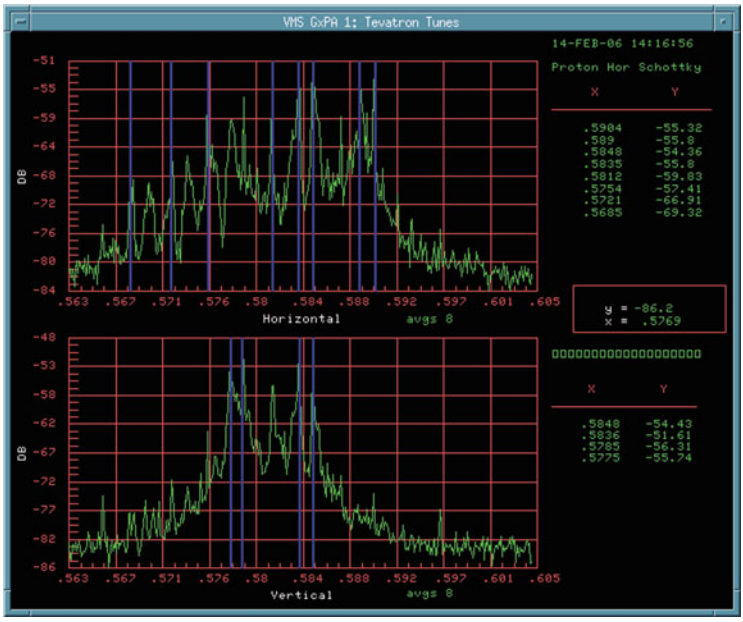

Fig. 9.7 Schottky spectra from the 21.4 MHz pickups. The spectrum typically contains many peaks, and it may be hard to determine which one is the tune. The system is also unable to resolve antiprotons, due to the much stronger proton signal [1]

Thus, in most practical applications the Schottky noise properties of the bunched beam are not much different from the case of continuous beam. If frequency is not sufficiently high ($f < \ln(N_p)/(2\pi\sigma_\tau)$), the coherent peak at the revolution frequency harmonics is well visible but does not distort the spectrum if electronics has sufficient dynamic range. Here σ_τ is the rms bunch duration. However, in the case of intense beams a small amplitude coherent longitudinal motion can persist for very long time (many hours in the case of normal colliding bunches in Tevatron at 980 GeV). In this case an observation of "true" Schottky noise requires significantly higher frequencies than is determined by the above estimate.

9.3.3 21 MHz Tevatron Schottky Detectors

There are several systems that measure tunes in the Tevatron. The 21 MHz Schottky monitor [12] is the workhorse for tune measurements during shot setup and studies. The tune is determined by the operator, looking at the Schottky spectrum on a signal analyzer in the Control Room—see Fig. 9.7. The result may be somewhat subjective, since the spectra typically contain numerous coherent peaks, and it may not be

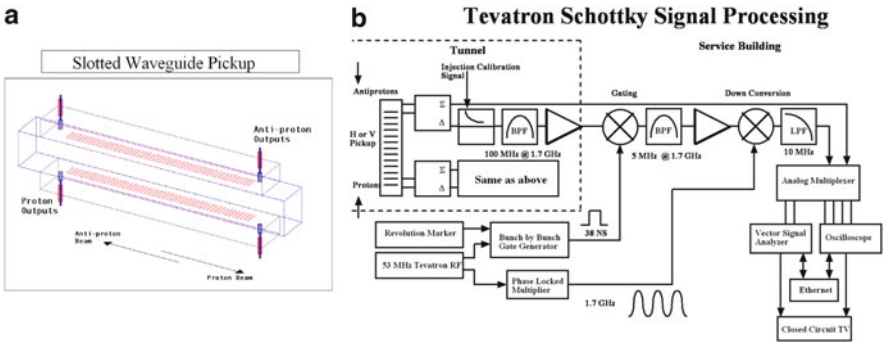

Fig. 9.8 (**a**) (*left*) Schematic of a 1.7 GHz slotted waveguide pickup. (**b**) (*right*) Schematic of the electronics and readout system [14]

immediately clear which one (if any) represent the real tune. To enhance the signal and make the tunes visible, noise can be injected into the beam through the transverse damper system.

The 21 MHz Schottky system was originally designed with movable pickup plates to maximize sensitivity. The original incarnation also had two pickups which could be added with a variable phase to suppress the proton tune in favor of the antiproton tune, although the practical usefulness of this feature in operation was very limited. The pickups are resonant with a tunable resonance frequency. This was intended mainly to compensate for the change in capacitance when the plates were moved. In Run II, the plates are left in a fixed position, and hence tuning is only done occasionally. The 21 MHz Schottky system is used to measure the horizontal and vertical tunes of the proton beam (antiproton signal is attenuated by 20 dB) without the possibility of gating on individual bunches. It has high resolution of about 0.0001.

9.3.4 1.7 GHz Tevatron Schottky Detectors

The 1.7 GHz Schottky pickups [13] are slotted waveguide structures (see Fig. 9.8). The high operating frequency was chosen to be above the coherent spectrum of the beam, thus measuring "true" Schottky signals. Since the devices are not resonant, it is possible to gate on select bunches, making it possible to measure the antiproton tune in the presence of protons. Chromaticity, momentum spread, and emittance can also be extracted from the signals, making the 1.7 GHz Schottky a very versatile tool [14].

An advantage of these pickups is that they can be used to measure tunes during normal operation without additional beam excitation. In order to maximize the usefulness of these devices, open access client (OAC) software was developed to

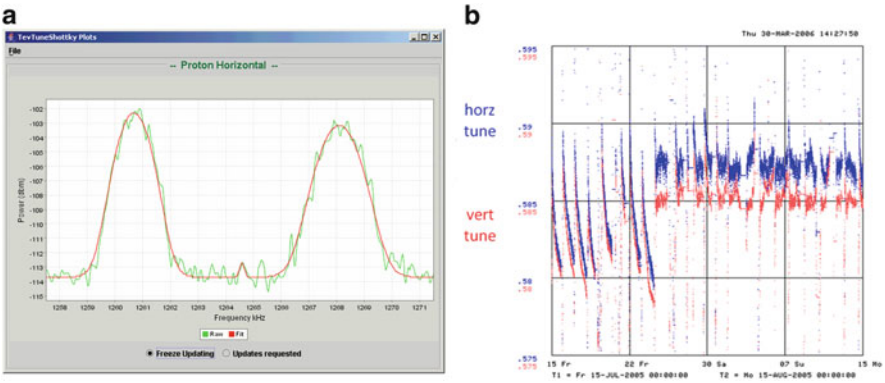

Fig. 9.9 (**a**) (*left*) Schottky spectra from the 1.7 GHz Schottky, showing both upper and lower betatron sidebands; (**b**) (*right*) Logged antiproton tune values over several weeks showing the effect of tune compensation during stores. Before the operators started using the 1.7 GHz Schottky tune readback to compensate for tune drifts, the tune would change significantly during a store as a result of the decreasing beam–beam parameter (*top line*—horizontal tune, *bottom*—vertical tune) [1]

run continuously, analyze the data, and publish the resulting tune, chromaticity, momentum spread, and emittance on ACNET. Among other things, this allows the tunes to be logged. The 1.7 GHz tune readings are also used in everyday operation to adjust the antiproton tunes as the beam–beam tune shift changes over the course of a store (see Fig. 9.9).

A peculiarity with the system is that due to the high frequency, the Schottky bands are very wide, and therefore it is not possible resolve the normal modes by frequency. The effect causes an underestimation of the tune separation in the presence of coupling (it can be shown that it approximately measures the uncoupled tunes). Though the 1.7 GHz Schottky monitors are capable of measuring the horizontal and vertical tunes of individual proton and antiproton bunch but to get to the precision of 0.0001, a few minutes of averaging time is required.

One of the original reasons for developing the system was to be able to extract emittance from the Schottky spectrum during stores. However, it has been observed that even in the microwave range, the Schottky spectrum still has a significant coherent contribution. The reason for this has yet to be fully understood. In the meantime, new thinner carbon filaments have enabled the use of the "flying wires" (see below) during stores, reducing the need for Schottky pickups for this particular task.

Identical 1.7 GHz Schottky detectors are used to monitor the betatron band power of the 8 GeV antiproton beam in the Recycler ring. The computed betatron power is scaled to reflect the transverse emittance of the beam based on the constants obtained from calibration with the mechanical scrapers.

9.4 Other Tune Diagnostics

9.4.1 Digital Tune Monitor and Tunetracker

It has been estimated that the beam in the Tevatron oscillates with ≈0.1 μm amplitude at betatron frequencies; at lower frequencies, the oscillation amplitudes can be larger ~1–10 μm due to various noise sources, not all well known, including ground motion, jitter in magnet and separator power supplies, and vibrations from the cryogenic system (see Sect. 2.4). In an attempt to use this effect to measure the tune without excitation, a very sensitive system called Digital Tune Meter (DTM) has been developed. This system is quite similar to the 3D-BBQ (Direct Diode Detection Base Band Tune) system developed at CERN in that it uses a diode-based sample and hold circuit, but it includes some novel features. Rather than measuring only the positive or negative peak from a stripline doublet, it measures both and takes the difference. It also employs slow feedback to remove baseline variations that can be quite large, thus enhancing the dynamic range. Fourier transformation of the position signal allows to determine the tune. The RMS position resolution of the DTM in the FFT averaging mode was estimated to be of the order of 100 nm. The averaged spectra for all 36 individual bunches are available from the DTM in about 80 s (2.2 s are required to record 25 sets of 4,096 turns [15]). The DTM has been successfully tested with proton beam, showed very good tune resolution for individual bunches of about 0.0002 at a low level of beam excitation by external noise, and has been used during dedicated beam studies [16].

The Tunetracker system uses a phase-locked loop (PLL) around the beam response. The beam is excited at a given frequency using a stripline pickup as a kicker, and the response is measured on another stripline. The PLL locks to a given frequency in the tune spectra, defined by a pre-selected phase response value, and tracks any changes in the tune. A typical tune tracking rms error is of about 0.0003–0.0006. A novelty in the Tevatron system compared to previous tune tracker implementations is the capability of pulsed excitation. When measured with high resolution, the beam phase response exhibits large excursions from the synchrotron sidebands, which can cause the PLL to jump from one synchrotron band to another. By pulsing the excitation, the measured phase response is smoothed out to follow the slow underlying phase response more closely, resulting in a more reliable measurement [17].

9.4.2 Tune Measurements from Turn-by-Turn Data

Tune determination from turn-by-turn beam position measurements after a transverse kick still remains the most reliable diagnostics in many Fermilab accelerators. In fast ramping synchrotrons like the Fermilab Booster the conventional method of

betatron tune evaluation does not work due to rapid changes of the tunes (sometimes in a course of a few dozens of turns) and a high level of noise. Standard method for tune evaluation using fast Fourier transform (FFT) has resolution ~$1/N$, N being the number of turns, which is insufficient in the case of rapid changes of the tunes and/or fast decoherence of the betatron oscillations. Much better precision can be achieved with the so-called Continuous Fourier Transform (CFT) method [18] which consists in evaluation of the sum:

$$X(\nu) = \frac{1}{N}\sum_{n=1}^{N} x_n e^{-2\pi\nu(n-1)} \tag{9.35}$$

as a function of continuous variable ν and finding the maximum of $|X(\nu)|$. In absence of random noise CFT provides precision ~$1/N^2$. There are methods—i.e. the Hanning windowing technique—which further improve precision, up to $1/N^4$, but they fail in the presence of noise. In the case of white noise the CFT provides tune with the r.m.s. error of $\sigma_\nu \approx \frac{\sqrt{6}\sigma}{\pi N^{3/2} a}$ where σ is the r.m.s. value of BPM errors and a is the betatron oscillations amplitude, which is better than the FFT error even in absence of noise. But it may be still not enough in a situation when the noise level is high and only a small number of turns are available.

A new technique based on phasing of signals from a large number of BPMs which significantly increases the signal to noise ratio has been proposed in [19] and implemented for routine operational use in the Booster. The turn-by-turn position data from many (all) BPMs are used to construct a phased sum (phasor)

$$\widetilde{x}_n = \sum_{k=1}^{N_{\mathrm{BPM}}} x_n^{(k)} \mathrm{e}^{-i\varphi(k)} \tag{9.36}$$

where k being the BPM index and $\phi(k)$ is the betatron phase advance between. It was shown that the phase advances from a theoretical optics model can be used as effectively as real measured ones. Performing the CFT analysis of the phased sum gives the tune value. One can easily see that the proper part of the signal propagating with expected phase advance is amplified by a factor of N_{BPM} whereas the alien modes and random noise are amplified only as $\sqrt{N_{\mathrm{BPM}}}$ so that the signal to noise ratio is improved by a factor of $\sqrt{N_{\mathrm{BPM}}}$.

In the Booster, a kicker—horizontal or vertical—is set up to kick the beam every 500 turns. On completion of the ramp the application reads out the turn by turn BPM data for all turns and all BPM's. The horizontal or vertical BPM's readings are then combined for each turn according to Eq. (9.36) and the moments of pings on the beam are identified by the oscillation. CFTs are then performed for each ping. Each spectrum is normalized so that the peak value is the same for all pings. Figure 9.10 compares contour plots of the CFT spectra obtained from a single BPM and from the phased sum. The achieved clarification of the spectra allowed

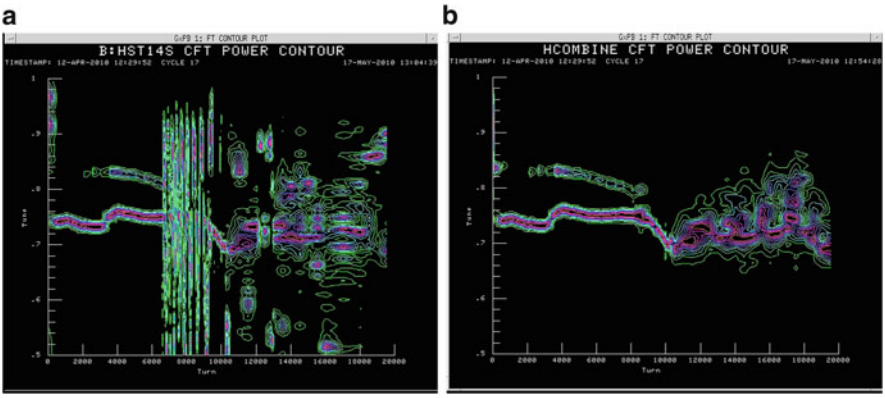

Fig. 9.10 (**a**) (*left*) Contour plot of the CFT spectra of the horizontally pinged beam obtained from one BPM; (**b**) (*right*) Contour plot of the CFT spectra of the phase-combined sum from 24 BPMs [19]

better tuning of the Booster which resulted in noticeably improved performance. The remaining fuzziness in the second part of the ramp is a result of systematic noise probably produced by the BPM electronics.

9.5 Data-Logging and On/Offline Presentation

Online and offline access to the vast amount of accelerator data is crucial to evaluating and improving machine performance and diagnosing failures. Retaining bunch-by-bunch values is especially useful since the beam dynamics vary over the bunch positions within a train. In the Tevatron collider complex, the readings and settings of accelerator devices are obtained via Fermilab's own ACNET control system. Device data can be plotted live at up to 1,440 Hz. Device data can be logged at various fixed rates or periods, e.g. 15 Hz or 1 min, or on a specific event, e.g. when the energy ramp is complete. Logged data is stored in circular buffers on ~70 nodes hosting a MySQL database and ~80 GB of storage for compressed data. The data in the circular buffers wrap-around in a time that depends upon the number of devices and their logged rate for a given logger. Logged data up to a 1 Hz maximum rate is also copied to a "backup" logger for long-term storage.

There are several means of accessing and plotting accelerator data: standard C-language based console applications used in operations, Java applications via a web-based interface, exports to Excel spreadsheets and Java Analysis Studio files, as well as programmatic APIs. Each method has its own advantages and disadvantages, but the flexibility allows users, both on-site and off-site, to access the data

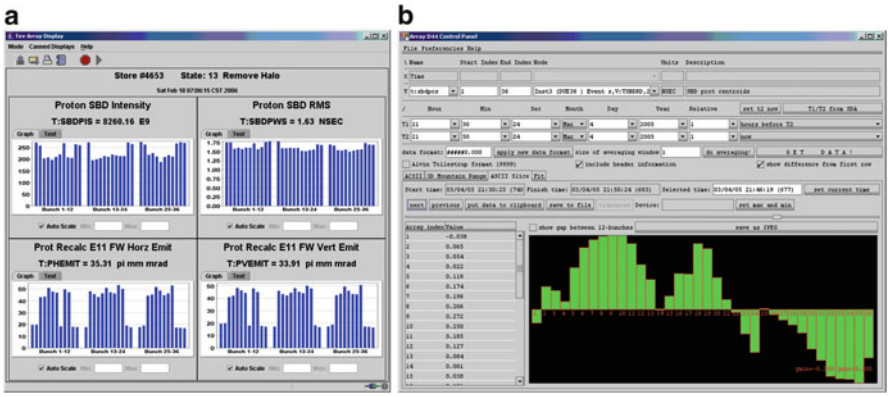

Fig. 9.11 (**a**) (*left*) The window of a Java applications showing live, bunch-by-bunch data for Tevatron proton bunches including intensity, RMS bunch length, and transverse emittances; an instability during antiproton injections had caused emittance growth and beam loss for particular proton bunches. (**b**) (*right*) A Java application showing a snapshot of logged proton bunch centroid positions within their RF buckets; a longitudinal, coupled-bunch instability with $\pm 4^\circ$ of RF phase oscillation amplitude was occurring at the time [1]

how they want or need. Figure 9.11 shows two examples of accessing Tevatron data.

In addition to the above data-logging scheme, data for all Tevatron shots is automatically collected and stored via a package called SDA, for Sequence Data Acquisition. The desired data and plots for all stages of a shot (injection, low-beta squeeze, etc.) can be easily configured. SDA also stands for Shot Data Analysis; SDA software automatically generates summary reports and tables for each store. These data are readily accessible by various means and allow for convenient analysis of the accelerator complex on a shot-by-shot basis [20].

9.6 Longitudinal Beam Diagnostics

The Tevatron resistive wall current monitors (WCM) [21] consists of a short ceramic vacuum pipe with 80 resistors across it. A copper casing around the ceramic break filled with ferrite provides a low impedance bypass for DC currents while forcing AC currents to flow through the resistors. There are also ferrite cores inside the vacuum to improve the signal quality. With the larger number of bunches and higher intensities, the resistive wall monitors developed vacuum problems early in Run II. The cause was beam-related heating of the ferrite cores. This problem was solved by replacing the ferrite with a different type. Signals from four locations around the ceramic pipe are summed to provide an intensity measurement. There are two resistive wall monitors in the Tevatron. One is dedicated to the Fast Bunch Integrator (FBI) and

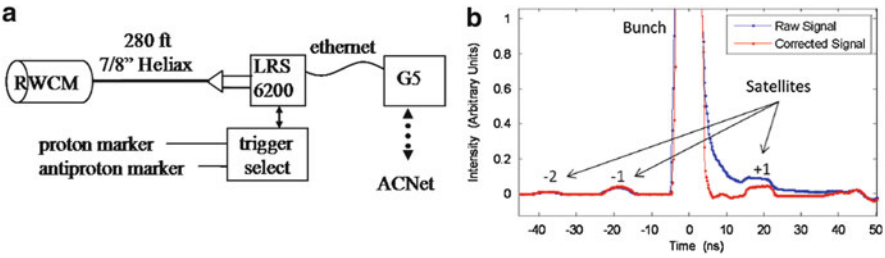

Fig. 9.12 (**a**) (*left*) Schematics of the signal acquisition from resistive wall current monitor. (**b**) (*right*) Raw and corrected signals for a Tevatron proton bunch and satellites. One can easily see the effect of removing the dispersion [1]

Sampled Bunch Display (SBD), and the other is for general use. This is to avoid errors in intensity readings due to improper terminations.

The schematic of the Tevatron SBD [22] is shown in Fig. 9.12a. The source of the signal is a wide-band resistive WCM installed in the F0 straight section of the Tevatron which also houses the RF cavities. In the Tevatron, since protons and antiprotons circulate oppositely within the same beampipe, the WCM is located at F11 where the proton and antiproton bunches are maximally separated (~30 m from the center of the straight section). The WCM has a >4 GHz bandwidth with a ~1 Ω gap resistance. The WCM signal travels from the tunnel to an above ground service building through a 7/8 in. Heliax cable. There it is split and digitized by two separate channels of LeCroy Corporation Wave Runner 6200 series digital scope having a 2 GHz bandwidth and 5 GSamples/s sampling rate. The splitter produces two identical signals which are captured by high-gain and low-gain channels in the oscilloscope that allows to effectively increase the dynamic range. In the Tevatron, where the coexisting protons and antiprotons vary in intensity by more than a factor of 3, the disparate gains allow simultaneous measurements of both particle species with equal sensitivity. The oscilloscope trigger generation is controlled by a separate board which is programmed to send 64 triggers to the oscilloscope, once every other revolution. The first 32 are triggered by the proton beam marker and the second 32 are triggered by the antiproton beam marker to obtain the relative antiproton timing. After digitizing the total number of beam revolutions, the digitized data is sent to an Apple Mac Pro computer for signal processing (combining of the 2 different gains to form one signal, correction of the dispersion in the cable from the WCM to the oscilloscope, and subtraction of the baseline) and extraction of longitudinal beam parameters (individual bunch intensity, the mean phase and rms width, the skew and kurtosis, and the emittance and momentum spread). All the processing is done within the National Instruments LabVIEW framework and the results are made available to the Accelerator Controls Network (ACNet) once a second continuously.

The longitudinal phase monitor (LPM) [23] is using the signal from a stripline pickup. The original idea was to use the antisymmetric shape of the bunch signal

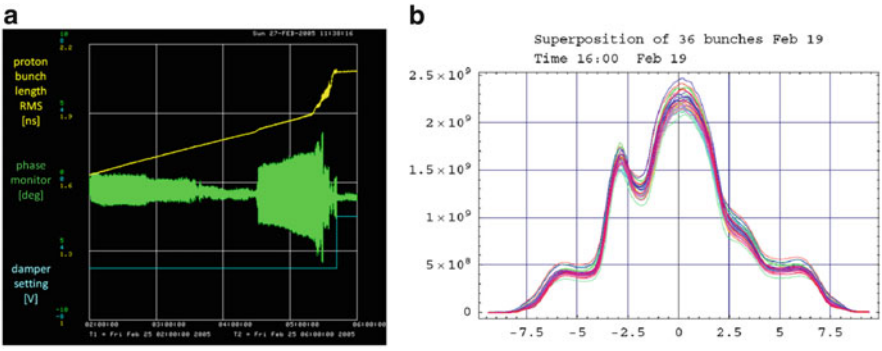

Fig. 9.13 (**a**) (*left*) Longitudinal phase monitor readings during an instability. (**b**) (*right*) Shapes of all 36 proton bunches as detected by the Tevatron SBD after longitudinal instability had developed [1]

from a stripline pickup, by multiplying it with a sine and cosine function locked to the RF. The two signals are then integrated over the bunch, and the phase can be extracted from the ratio of the two integrals. This was implemented in analog electronics using mixers and gated integrators, and the result was digitized and processed in an FPGA. The FPGA calculated the average over all bunches and output it as an analog voltage through a DAC. Turn-by-turn values were also saved in buffer memory and could be retrieved via an Ethernet interface (Fig. 9.13).

9.7 Abort Gap Monitors

Longitudinal instabilities, RF noise, and intra-beam scattering can cause particles to leak out of RF buckets and into satellites or into the abort gaps [24, 25]—see Fig. 9.14. There are three 2.6 μs gaps between 3 trains of 12 bunches each separated by 396 ns. The presence of even a small fraction (few 10^9 or 0.0001 of the total) of the beam in the abort gaps can induce quenches of the superconducting magnets, as these particles are sprayed onto the magnets when an abort kicker fires, and inflict severe radiation damage on the silicon detectors of the CDF and D0 experiments. Synchrotron radiation (SR) from these unwanted 980 GeV protons is collected for monitoring their intensity.

A very sensitive gated monitor of the SR from the beam in the gap was developed on the base of Hamamatsu R5916U-50 micro-channel plate (MCP) PMT with a minimum gating time of 5 ns. This tube can be used to measure DC beam intensity immediately following a bunch of protons. The DAQ system consists of a fast integrator, to which the anode of the PMT is connected, and a VME digitizer that is read by an application on a processor board residing in the

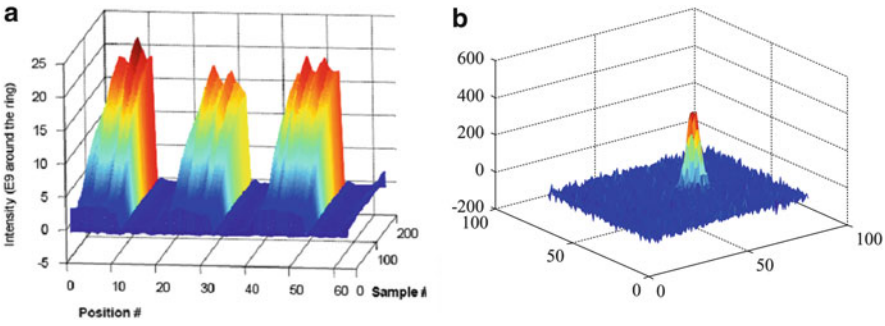

Fig. 9.14 (**a**) (*left*) Time evolution of beam in the gaps and between main bunches during a store (sample #200 corresponds to about 20 h, position # reflects 340 ns gap synchronization with respect to the revolution marker. Intensity is given in the units of equivalent number of particles if uniformly distributed around the circumference). (**b**) (*right*) Profile of DC beam in the gap imaged by a CID camera [1]

VME crate. Data is collected for 1,000 revolutions and averaged in the processor board. This cycle is repeated every 3 or 4 s. The application controls the timing of both the PMT and integration boards. Figure 9.14a shows how the intensity of the beam outside of the main 36 bunches is growing over a course of a HEP store. A standard synchrotron light monitor equipped with an image intensifier can see the DC beam profile, but only if enough camera frames can be summed together. A LabVIEW-controlled Windows PC system does such integration of CID camera RS-170 video images captured by a frame-grabber card. Figure 9.14b presents an example of the proton DC beam profile in the Tevatron. Details of calibrating and measuring the intensity of beam in the abort gap using synchrotron light and a gated photomultiplier tube can be found in [26].

9.8 Intensity Measurements

In the Tevatron, a DC Current Transformer (DCCT) and a Resistive Wall Current Monitor (RWCM or RWM) are the pieces of instrumentation that allow beam intensity measurements [27, 28]. The DCCT can only provide a measurement of the total beam intensity (sum of proton and antiproton currents). The RWM does distinguish between protons and antiprotons because of its high bandwidth and location where the protons and antiprotons are well separated in time.

The DCCT front-end contains an Interactive Circuits and Systems (ICS) ICS-110BL-8B 24-bit, 8-channel ADC to digitize the DCCT signal and a Motorola MVME-2401 processor. The ADC samples at 6.9 MHz and outputs a 128-sample average measurement at 54 kHz. The crate CPU performs additional averaging and

provides the interface to ACNET. There is also a circular buffer that can be stopped upon a beam abort in order to help diagnose the cause of beam loss. The DCCT provides the most precise intensity measurements with a resolution of $\approx 0.5 \times 10^9$ for typical Tevatron total beam intensities of 10^{11}–10^{13} particles. The DCCT is calibrated via an external pulser.

Bunched-beam intensity measurements are made by the FBI and SBD systems, both of which use the RWM as their signal source. The FBI uses ADCs to integrate the RWM output gated on the individual RF buckets and obtain baseline measurements taken in the gaps between each train. A Motorola MVME-2401 processor performs the baseline correction and acts as the interface to ACNET. The FBI system provides narrow-gate (single bucket) and wide-gate (five buckets) intensity measurements for all proton and antiproton bunches at a rate of up to a few hundred Hz. Comparing the narrow and wide-gate values provides a measure of the intensity of satellite bunches, typically a few percent of the main bunch intensity.

The SBD configuration was described previously. The resolution of the bunch intensity measurements is $\approx 0.5 \times 10^9$ for present typical intensities of 20–80 $\times 10^9$ for antiprotons and 240–300 $\times 10^9$ for protons. The SBD can update measurements at approximately 1 Hz rate.

Both the FBI and SBD intensities can be calibrated via the very well-known measurement provided by the DCCT via the equation:

$$I_{\mathrm{DCCT}} = I_{\mathrm{P,true}} + I_{\mathrm{A,true}} = I_{\mathrm{P,RWM}} \times \left(1 + \frac{I_{\mathrm{A,RWM}}}{I_{\mathrm{P,RWM}}}\right) \times A_{\mathrm{calib}}, \tag{9.37}$$

where the DCCT intensity should be equal to the sum of the measured bunch intensities. A few percent correction needs to be made for satellites and other beam observed by the DCCT but not the FBI or SBD. This method requires no knowledge of the RWM, but only the relative gains of the proton and antiproton channels of the system being calibrated.

9.9 Beam Loss Monitoring System

Careful diagnostics and control of beam losses is crucial for the operation of the collider. Beam-Loss Monitors (BLM) are installed at each quadrupole magnet and at a number of critical components. The physical particle detector is an Ar-filled glass cylindrical ionization chamber with nickel electrodes and was chosen to be extremely radiation hard [29]. The gas is 1 atm pure Ar with an active volume about 110 cm^3. No CO_2 was used, because CO_2 could eventually dissociate under ionizing radiation and alter the response. The detector calibration is 70 nC/Rad and is extremely stable. The ionization chamber design was a compromise among high gain, fast response, size, and low cost. The design included placing the anode

(center electrode, positive high voltage) and cathode (outer electrode, signal) feedthroughs at opposite ends of the glass bottle with a guard ring on the glass envelope to minimize the dark current leakage (roughly 100 pA at 2,500 V). Pulsed-beam measurements at Argonne National Lab showed that the chamber could detect an instantaneous radiation dose (in 1 or 2 μs) of about 10 Rads with less than 20 % charge loss. This large amount of space charge (about 700 nC) severely modifies the electric fields in the gas as the ions and electrons drift toward the electrodes, leading to both recombination losses and gas multiplication. For comparison, the inter-electrode capacitance is about 2 pF, leading to a displacement charge on the electrodes of about 5 nC at 2,500 V. The signal from the cathode is brought out of the tunnel enclosure on RG-58 cable, which is not particularly noise resistant. Complicating the noise situation is the legacy high voltage distribution which is supplied via a single RG-58 cable daisy chained through typically 12 ionization chambers producing myriad ground loops with the signal cables. Additionally, noise sources vary depending on the location within the accelerator. To combat the noise conditions, a variety of schemes are utilized to reduce the noise pickup to acceptable levels. An inductive choke is used on each signal cable just before the acquisition electronics to reduce large common-mode noise pickup on the cable. The size of the choke was chosen to give the proper frequency response. In parallel with the hardware efforts at noise reduction, a software algorithm was developed to subtract coherent noise from the signal in cases where the analog noise rejection techniques were insufficient [30].

The original BLM system ca 1980s was not adequate to the challenges of high luminosity Collider Run II operation, the BLM system was disabled during collider operation and protection of the Tevatron magnets relied on the quench protection system. In 2008, it was replaced by a sophisticated VME-based data acquisition system [30] which allowed appropriate abort logic and abort thresholds on losses to be set over the full set of collider operating conditions. The upgrade also provided better post abort diagnostics through its turn-by-turn buffer and the three buffers of integrated loss types. The upgrade has proven to be robust resulting in less downtime and maintenance requirements.

9.10 Chromaticity Diagnostics

High intensity proton and antiproton beam stability and lifetime depend strongly on machine chromaticity [31]. So, one of the operational challenges in the Tevatron is to measure accurately and control both vertical and horizontal chromaticities so that they are high enough to keep beam stable, yet low enough to avoid high beam losses. Several methods are employed.

The standard one—observation of the tune change while changing RF frequency—works well and is accurate to ~0.5 unit of Q' with ± 40 Hz change of the $f_{RF} = 53.1$ MHz if measured by 21 MHz Schottky tune detector. A much faster,

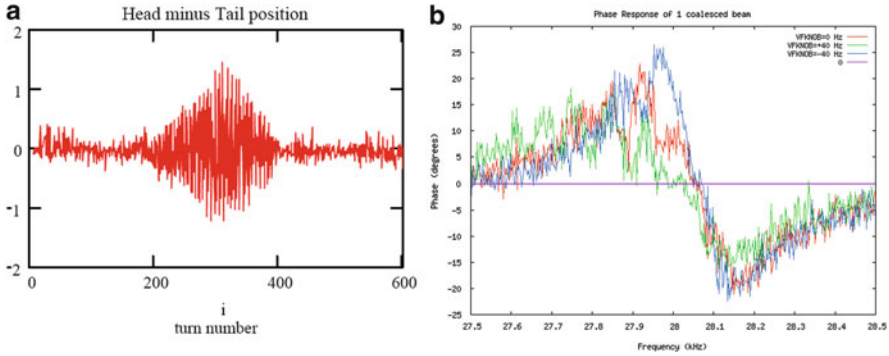

Fig. 9.15 (**a**) (*left*) Differential motion (in mm) between the head (+4 ns off bunch center) and tail (−4 ns) of a high intensity proton bunch in the Tevatron at 150 GeV vs turn number after a 1 mm vertical kick. (**b**) (*right*) Tune Tracker Beam Response Function spectra measured with $\approx 200 \times 10^9$ per bunch at 150 GeV, the zero-crossing frequency (betatron frequency) varies with the RF frequency change of ±40 Hz

but just as accurate head-tail method has been developed [32]. In that method, beam is kicked (causing a slight ~5 % emittance growth) and the differential motion of bunch head and bunch tail, as measured by a stripline pickup, is recorded by a fast digital scope (Tektronix TDS7000, 1.5 GHz analog bandwidth, 5 GS/s). An example is shown in Fig. 9.15a. The amplitude of the motion has a maximum at half of the synchrotron period (about 300 turns in Fig. 9.15a), and is proportional to Q'. Chromaticity found by that method agrees with the RF method to within ~±0.5 unit. Another fast and even less destructive technique is to take advantage of the superb accuracy and precision of the Tune Tracker for the RF method. Figure 9.15b shows BTF function measurements with the TT for different RF frequencies—again, chromaticity can be found from the tune shift as $Q' = -dQ/(df_{\mathrm{RF}}/f_{\mathrm{RF}})/\eta$, where $\eta = 0.00283$ is the Tevatron lattice momentum compaction factor. The tune measurement accuracy is better than 0.0001 with 3 Hz bandwidth, resulting in Q' accuracy of about 0.2 units. There are systematic Q' differences of about 0.5 unit between the three methods which are due to the second-order chromaticity induced by octupoles.

9.11 Beam Profile Monitors

9.11.1 Flying Wires

The so-called Flying Wires [33] have been the main source of determining transverse emittances and profiles of the protons and antiprotons. There are three flying wire cans in the Tevatron: one horizontal and one vertical at a low dispersion area,

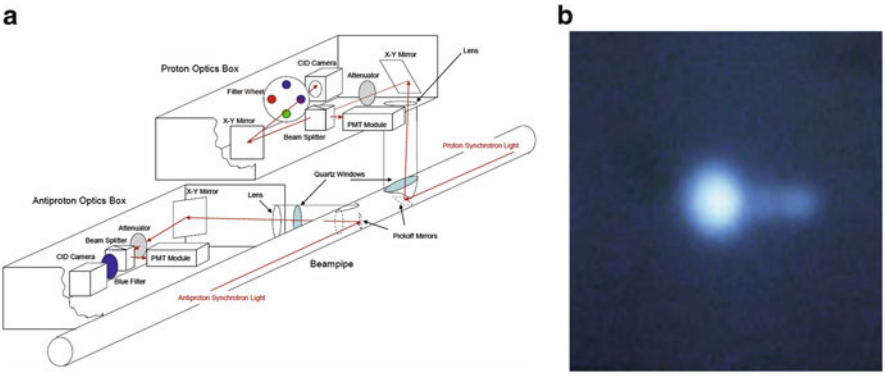

Fig. 9.16 (**a**) (*left*) 3D view of the SyncLite systems; (**b**) (*right*) Image of the synchrotron light emitted by 980 GeV antiprotons; the peak on the left is the dipole edge radiation which is used for beam size calculations, the tail on the right is radiation from the body of the magnet which is omitted in the image analysis [34]

and one horizontal at a high dispersion location. The original flying wire cans had 33 μm diameter carbon fibers, but those thick wires caused high loss spikes in the experiments when they were used during HEP stores and therefore were of limited use. Since the original fibers were changed to 5 μm, the wires are used routinely in every stage of operation. Wires are flown following most proton injections, after each pbar injection, several times during ramp, squeeze and halo removal (scraping), and every hour during HEP stores. The flying wires provide the rms normalized emittance measurements with about 0.2 π mm mrad uncertainty. Uncertainties in the lattice parameters at those locations were a major systematic error for the emittance measurement. Similar Flying Wires systems are also in daily operation in the Main Injector (one vertical and one horizontal), and in the Recycler ring (one vertical and one horizontal).

9.11.2 Synchrotron Light Monitor

The synchrotron radiation emitted by protons and antiprotons from the edges of the Tevatron dipoles is enhanced in the blue optical region, one can point a telescope at it and produce a transverse image of the beams. The Synclite system [34] does this and thus offers a nondestructive method for measuring the transverse beam emittances. For the Tevatron, synchrotron radiation is non-negligible only when the beam energy gets above 600–700 GeV. The physical layout of the Synclite system is shown in Fig. 9.16 and comprises a vacuum insertion mechanism to which is attached a pickoff mirror, and a light tight box containing the necessary optics for forming an image. The optical path contains a single lens for focusing, motorized

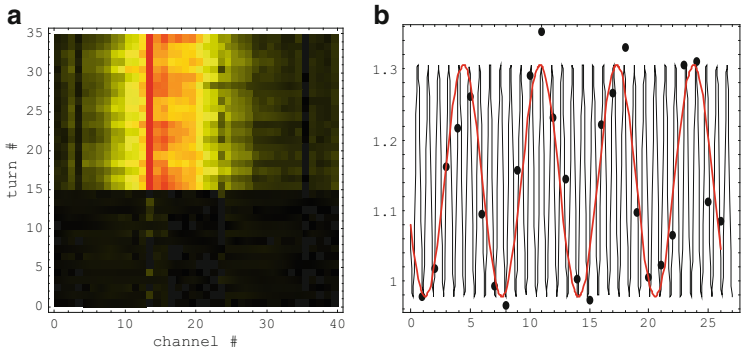

Fig. 9.17 (**a**) (*left*) TBT vertical profile of a coalesced proton bunch at injection using the IPM. The bunch was injected at turn #15 on this plot. This horizontal coordinate corresponds to ≈1 cm. (**b**) (*right*) Measured profile widths calculated from the turn-by-turn data. *Black dots* are IPM data, *red line* is a fit to $\cos((2\nu_y - 41)n)$, *black line* is a fit to $\cos(2\nu_y n)$ [1]

mirrors for positioning the image, a 440/10 nm band pass filter (400/40 nm for pbars), and a gated, Image Intensified CID (Charge Injection Device) camera for obtaining the image. The image is retrieved from a frame grabber in a PC running Windows XP and LabVIEW. The image has its background subtracted before the beam sizes are extracted from fits to the horizontal and vertical profiles in a window around the peak. The fits are simple Gaussians with linear baselines. The values of the fits are then corrected for nonlinearities in the intensified camera response and for theoretical distortions in the image (most notably, the broadening of the peak due to diffraction—the impact is about 100 μm on a beam size which for pbars is in the range of 200–400 μm—and the impact from the longitudinal extension of the source). Comparisons have been made with the profile measurements from the flying wires and reported emittances agree within ±10 % [35].

9.11.3 Ionization Profile Monitors (IPM)

The Tevatron IPM's [36] were designed to be single turn, single bunch devices, in order to resolve any turn-by-turn beam size oscillation caused by injection mismatch—see Fig. 9.17—as well as to allow noninvasive, nearly continuous measurement of the beam profiles at all stages of operation. The IPM data from multiple turns can be combined in software to create an average beam profile from which the emittance can be calculated. The IPM measures ionization electrons collected using a parallel electric and magnetic field. A localized pressure bump obtained by controlled injection of pure N2 is required to obtain single turn sensitivity. The magnets and gas injection is left on continuously, while the high voltage sweep field is pulsed only for acquisitions. The detector granularity is

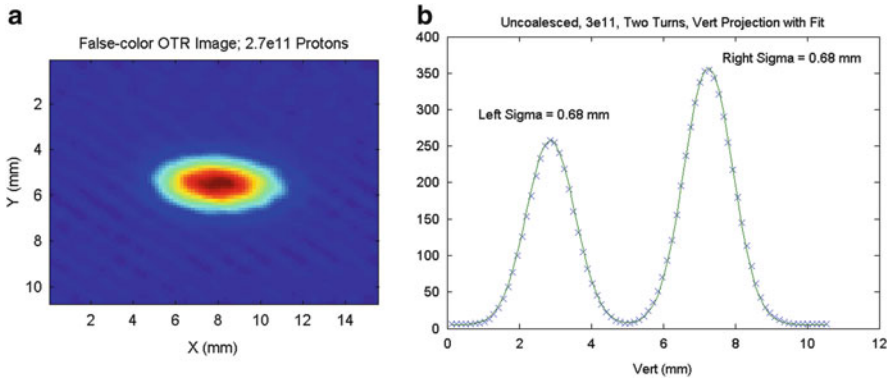

Fig. 9.18 (**a**) (*left*) Transverse 2D bunch profile as measured by the OTR. (**b**) (*right*) Vertical profiles of a single proton bunch from the OTR on two consecutive turns. The second turn profile is offset from the first, and the images are summed together by the slow camera. Note that over the two first turns, the OTR does not show evidence of the quadrupole oscillations seen in the IPM. However, from the IPM data only a 5 % effect is expected between these two turns [1]

1/4 mm, and the readout uses electronics borrowed from HEP experiments, enabling close to single electron sensitivity. Similar IPM systems but without bunch-by-bunch diagnostics capability are used for the emittance measurements in the Main Injector and Booster.

9.11.4 Optical Transition Radiation Detector

The Optical Transition Radiation (OTR) instrument [37] was installed close to the Tevatron IPM and used as a cross-check of the IPM at injection; we cannot leave the OTR foils inserted for routine operation as they tolerate only a few turns of beam. The OTR could also in principle be used for multi-turn acquisition, but the camera that is currently used does not have enough time resolution. However, by injecting a mis-steered beam, non-overlapping profiles from the two first turns can be obtained (see Fig. 9.18).

9.12 Special BPMs

9.12.1 Injection Beam-Line Tuners

To reduce emittance dilution caused by mis-steering at injection, dipole corrector magnets are adjusted by a beam-line tuner system, based on measurements of turn-

by-turn orbit positions from directional stripline pickups. The 1 m long striplines are separated by an 83 mm gap, have ≈30 dB directionality and 0.65 dB/mm sensitivity. Measurements from one injection are used to make corrections for the subsequent shot, and usually injection offsets can be reduced from 1 mm to less than ¼ mm. Measurements of synchrotron oscillations can be used to correct energy and RF phase differences between the Main Injector and Tevatron. In addition, the tunes and coupling at injection can also be extracted from the stripline signals. Two different beam-line tuners have been used. In the first, a Tektronix TDS7104 oscilloscope digitizes the sum and difference signals from the striplines, and the embedded PC performs the signal processing. That system has been used only for closure of antiproton injections; it was too slow for the more frequent proton injections. A faster system, based on the Struck SIS3300 digital receiver module, provides 20–40 μm position measurements for 1,000 turns [38]. The digitized data is transferred to a PC which performs digital down-conversion at 30 MHz and calculates the positions and time-of-arrival for the transferred bunches. This system can be used for both proton and antiproton injections. During stores, it can also continuously store position data into a circular buffer that is stopped on a beam abort. The buffered data can be used in the postmortem diagnosis of a lost store.

9.12.2 AC Dipole

An AC dipole is a magnet with a field oscillating close to the betatron frequency. By exiting the beam close to a resonance, a relatively small field can drive a large amplitude oscillation, and keep the oscillation amplitude constant over many turns—as demonstrated in Fig. 9.19—allowing precise measurements of the beam response without any emittance blow-up. Dedicated AC dipole magnets have been built before, e.g. for RHIC. In the Tevatron, an existing vertical “pinger” magnet was converted to a resonant circuit using an external capacitor bank, and driven by a commercial high-power audio amplifier. While very successful R&D project, both demonstrating the use of commercial audio equipment for this purpose and furthering the understanding of the analysis of driven oscillation data to extract the beam optics [39, 40], much like the kicked beam method, the AC dipole in the Tevatron has not been used much in operation. This is partially due to the fact that the system only measures one plane, but to a larger degree it is due to the success of the orbit response method. However, the tests performed in the Tevatron were carried over to the LHC, where a very similar system (based on audio amplifiers and resonant kicker magnets) is the prime method for measuring optics [41].

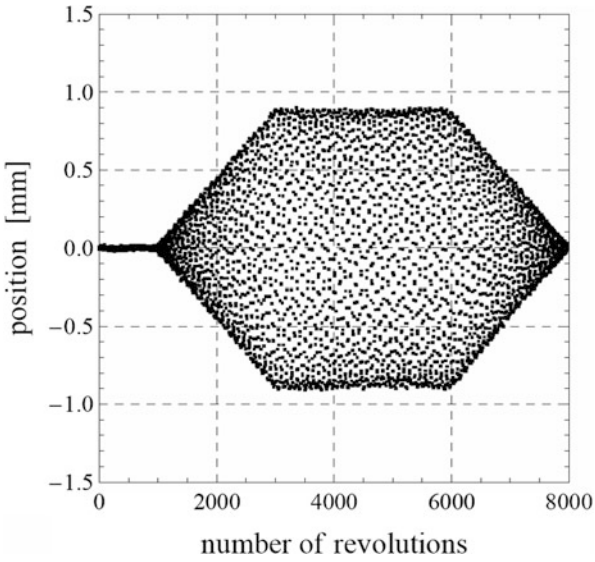

Fig. 9.19 Measured turn-by-turn oscillations of the beam driven by an AC dipole in the Tevatron. In contrast to a kicked beam, the driven particles do not lose the coherence. By adiabatically ramping up and down the amplitude of the AC dipole's field, an excitation is produced without increasing the beam size [39]

9.13 Discussion on the Beam Diagnostics for Tevatron Collider Accelerators

Development of many new diagnostic tools for the Tevatron Collider accelerators was needed to provide insights into serious issues of coherent instabilities, beam losses, and beam–beam interactions. As a result, almost two dozen various instruments were either developed or significantly improved, and that eventually paid off in the integrated luminosity delivered to the CDF and D0 detectors.

There are several lessons learned during this campaign. First, we realized the importance of multiple instruments for cross-checking and cross-calibrating one another. For example, there are several instruments to measure beam intensity: DC Current Transformer (DCCT), FBI, and SBD. The DCCT is the most precise but it has limited application range, e.g. it cannot report individual bunch intensities. The FBI and SBD are not as precise but they are really multi-functional, operating on a bunch-by-bunch basis, and calibrating them within 1 % of the DCCT made them trustworthy and very useful in operations. In addition, the fast LPM was cross-checked with the SBD. Three tune monitors—21 MHz Schottky (used for injection tune-up), 1.7 GHz Schottky (most versatile) detectors, and Tune Tracker (the fastest and most precise of the three)—are employed in operations for different tasks after being carefully cross-calibrated. A lot of effort over many years was needed to bring the three emittance measurement tools—Flying Wires (FWs), Synchrotron Light Monitor (SyncLite), and 1.7 GHz Schottky detector—into satisfactory agreement; currently, they agree within ± 5 %.

Another lesson is the need for noninvasive beam diagnostics for nearly continuous monitoring of beam parameters. The lack of any natural damping in proton

accelerators and the sensitivity of SC magnets to beam losses (quenches) restrict the use of invasive techniques that often have better resolution than noninvasive ones. For example, flying wires is the most precise and understood technique for emittance measurements, but the resulting background spikes and emittance growth limit their use to only once per hour during high-energy collision stores. The complementary, noninvasive Synchrotron light monitor and 1.7 GHz Schottky can report measurements every second.

A third lesson is that the Collider operation team needs fast data collection rate of all diagnostics and control channels (at least 1 Hz) for all channels at all stages of the machine cycle for all bunches all the time—and the data should be saved forever (for years)! That greatly helps to correlate machine behavior now with the past.

We have learned the usefulness of fast access to beam-related information that can be provided by the experimental detectors (CDF and D0, in our case), so good communication between the accelerator and experiment control systems and personnel is important. The luminous region parameters information noted above is a good example.

We also have benefited from help and ideas from other groups and laboratories that have expertise in a number of specific areas: for example, Fermilab's Computing Division experts took a leading role in development of DAQ for the Tevatron BPM upgrade; FNAL Particle Physics Division leads Tevatron BLM upgrade and provides luminous region analysis data (β^* monitors); Berkeley Lab contributed in the development of the MCP-PMT based Abort Gap Monitor, etc.

And finally, we realized that constructing a new instrument is fast compared to the time needed to make it "fully operational," i.e. satisfactory to operators and physicists. A lot of effort went into the debugging, tune-up, cross-calibration, and "polishing" of beam diagnostics. So, we teamed up diagnostics developers and users (physicists and engineers) from the very start of instrument development until the end of its commissioning. Such teams of two to four were very efficient in developing or overhauling about two dozen beam diagnostics instruments for the Tevatron Run II.

References

1. R.S. Moore, A. Jansson, V. Shiltsev, JINST **4**, P12018 (2009)
2. R.E. Shafer, R.C. Webber, T.H. Nicol, IEEE NS-28 **3**, 3390 (1981)
3. G. Annala et al., JINST **6**, T11005 (2011)
4. Yu. Alexahin, E. Gianfelice-Wendt, JINST **6,** P10006 (2011)
5. A. Petrenko, A. Valishev, V. Lebedev, Rev. ST Accel. Beams **14**, 092801 (2011)
6. V. Ranjbar, in *Proceedings of the 2005 IEEE Particle Accelerator Conference*, Knoxville, 2005, p. 1353
7. J.T. Volk et al., JINST **7**, P01004 (2012)
8. J. Slaughter et al., in *Proceedings of the 2003 IEEE Particle Accelerator Conference*, Portland, 2003, p. 1763
9. M. Jones et al., Preprint FNAL-TM-2172 (2002)
10. D. Boussard, CERN Accelerator School, CERN-Report 87-03 (1987), pp. 417–445
11. V. Parkhomchuk, D. Pestrikov, Sov. Phys. Tech. Phys. **25**(7), 818 (1980)

12. D. Martin et al., in *Proceedings of the 1989 IEEE Particle Accelerator Conference*, Chicago, 1989, pp. 1483 and 1486
13. R. Pasquinelli et al., in *Proceedings of the 2003 IEEE Particle Accelerator Conference*, Portland, 2003, p. 3068
14. R. Pasquinelli, A. Jansson, Phys. Rev. ST Accel. Beams **14**, 072803 (2011)
15. A. Semenov et al., *in Proceedings of the 2007 IEEE Particle Accelerator Conference*, Albuquerque, 2007, p. 3877; V. Kamerdzhiev et al., Preprint FERMILAB-CONF-08-139-AD-APC (2008)
16. V. Shiltsev, G. Stancari, A. Valishev, JINST **6** P08002 (2011)
17. C.Y. Tan, NIM A **557**, 615 (2006)
18. R. Bartolini et al., Part. Accel. **56**, 167–199 (1996)
19. Yu. Alexahin, E. Gianfelice-Wendt, W.L. Marsh, in *Proceedings of the International Particle Accelerator Conference*, Kyoto, 2010, p. 1179
20. T. Bolshakov et al., in *Proceedings of the 2005 IEEE Particle Accelerator Conference*, Knoxville, 2005, p. 1099; also T. Bolshakov, E.S. McCrory, in *Proceedings of the European Particle Accelerator Conference*, Edinburgh, 2006, p. 3101
21. J. Crisp, B. Fellenz, JINST **6**, T11001 (2011)
22. R. Thurman-Keup et al., JINST **6**, T10004 (2011)
23. J.P. Carneiro et al., in *Proceedings of the 2005 Particle Accelerator Conference*, Knoxville, 2005, p. 1428
24. X.L. Zhang et al., Phys. Rev. ST Accel. Beams **11**, 051002 (2008)
25. J. Steimel et al., in *Proceedings of the 2003 IEEE Particle Accelerator Conference*, Portland, 2003, p. 48
26. R. Thurman-Keup, in *Proceedings of the IEEE Particle Accelerator Conference*, Knoxville, 2005, p. 2440
27. S. Pordes et al., in *Proceedings of the 2003 IEEE Particle Accelerator Conference*, Portland, 2003, p. 2491
28. S. Pordes et al., in *Proceedings of the 2005 IEEE Particle Accelerator Conference*, Knoxville, 2005, p. 1362
29. R.E. Shafer et al., in *Proceedings of the XII International Conference on High Energy Accelerators*, Batavia, 1983, p. 609
30. A. Baumbaugh et al., JINST **6**, T11006 (2011)
31. P. Ivanov et al., in *Proceedings of the 2003 IEEE Particle Accelerator Conference*, Portland, 2003, p. 3062
32. V. Ranjbar, P. Ivanov, Phys. Rev. ST Accel. Beams **11**, 084401 (2008)
33. J. Gannon et al., in *Proceedings of the 1989 IEEE Particle Accelerator Conference*, Chicago, 1989, pp. 68–70; also in J. Zagel et al., in *Proceedings of the 1991 IEEE Particle Accelerator Conference*, San Francisco, 1991, pp. 1174–1176
34. R. Thurman-Keup et al., JINST **6**, T09003 (2011)
35. J. Zagel et al., in *Proceedings of the Beam Instrumentation Workshop BIW08*, Tahoe City, 2008, p. 282
36. A. Jansson et al., in *Proceedings of the Beam Instrumentation Workshop BIW06* (Fermilab), AIP Conference Proceedings 868, 2006, ed. by T. Meyer, R. Webberp, p. 159
37. V. Scarpine et al., in *Proceedings of the Beam Instrumentation Workshop*, AIP Conference Proceedings 868, 2006, ed. by T. Meyer, R. Webber, p. 473
38. W. Schappert et al., in *Proceedings of the 2003 IEEE Particle Accelerator Conference*, Portland, 2003, p. 2494
39. R. Miyamoto et al., in *Proceedings of the 2007 IEEE Particle Accelerator Conference*, Albuquerque, 2007, p. 3868
40. R. Miyamoto et al., Phys. Rev. ST Accel. Beams **11**, 084002 (2008)
41. R. Thomas et al., Phys. Rev. ST Accel. Beams **13**, 121004 (2010)